

Optimal Medial Surface Generation for Anatomical Volume Representations

Sergio Vera^{1,2}, Miguel A. González¹,
Marius George Linguraru³, and Debora Gil²

¹ Alma IT Systems, Barcelona, Spain

² Computer Vision Center, Comp. Science Dep.,
Universitat Autònoma de Barcelona, Spain

³ Sheikh Zayed Institute for Pediatric Surgical Innovation,
Children's National Medical Center, Washington DC, USA
`sergio.vera@cvc.uab.es`

Abstract. Medial representations are a widely used technique in abdominal organ shape representation and parametrization. Those methods require good medial manifolds as a starting point. Any medial surface used to parameterize a volume should be simple enough to allow an easy manipulation and complete enough to allow an accurate reconstruction of the volume. Obtaining good quality medial surfaces is still a problem with current iterative thinning methods. This forces the usage of generic, pre-calculated medial templates that are adapted to the final shape at the cost of a drop in volume reconstruction. This paper describes an operator for generation of medial structures that generates clean and complete manifolds well suited for their further use in medial representations of abdominal organ volumes. While being simpler than thinning surfaces, experiments show its high performance in volume reconstruction and preservation of medial surface main branching topology.

Keywords: Medial surface representation, volume reconstruction.

1 Introduction

One of the most used tools for volumetric shape representation are medial representations. In abdominal imaging, techniques such as M-Reps [9] and CM-Reps [19,18] have shown the potential to model complex anatomical shapes, and are being used in fields such as computational neuroanatomy [20,14], 3D cardiac modelling [15,16], and cancer treatment planning [12].

While other surface representation/parametrization methods model only the external surface of objects [2,3], medial representations can model also the interior of the shape by providing a radial perpendicular coordinate [1] that extends from the medial surface. This allows to parameterize the (possibly diseased) parenchyma of organs, and their internal vascular system, powerful sources of information in organ functionality, analysis and diagnosis. Any medial manifold used to (re)generate anatomical volumes must be simple enough to allow an

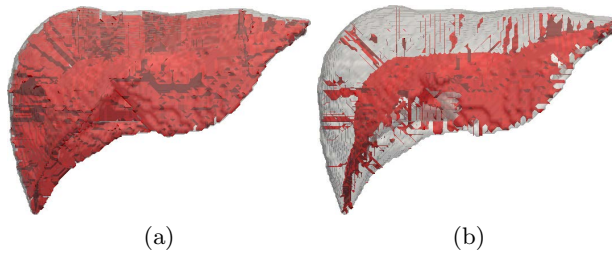


Fig. 1. Medial surfaces obtained using a 6-connected neighborhood (a), and a 26 connected neighborhood (b)

easy generation of the radial axis, but complete enough to allow a satisfactory reconstruction of the volume.

Most methods of medial surface computation are based on morphological (ordered) thinning operations on either the original volume or the distance map to its boundary. In any case, they require the definition of a neighborhood set and surface conditions for the removal of simple voxels (those that do not alter the topology if removed) that do not lie on a surface. The complexity of neighborhood definition and surface tests increases exponentially with the dimension of the embedding space [5]. Additionally, small changes in those tests or in the order in which voxels are traversed, generate completely different surfaces (as illustrated in Fig. 1). Surfaces produced with thinning based methods would need to be pruned in order to eliminate spurious branches and manifolds generated due to noise in the volume surface. However, there is no easy way to tell which manifolds can be safely removed without hurting the capability of representation of anatomical structures.

Some authors overcome this limitations using a generic manifold that has to be fitted into the volumetric shape [19]. This limits the number of objects that can be processed to those that can be represented by the topology of the template manifold. Simplified templates do not introduce a high reconstruction error as far as the concavity of the volume boundary keeps low (as for a number of subcortical brain structures [13]). However, anatomies with complex concavity patterns (such as abdominal organs [17]) or pathological shapes with severe deformation can not be captured by a deformed, simplified manifold.

Preserving the medial main branching topology is of prime importance for successfully applying medial representations to any anatomical shape. In order to do so, it would be desirable to generate specific initial manifolds for each anatomical case. This would remove fitting errors in the model and would capture the complete topology of volumes. Recent methods for medial surface generation based on Non Maxima Suppression (NMS) of medialness maps [17] have shown a strong potential to generate surfaces with minimal branching and great reconstruction power. In order to produce complete surfaces, the definition of the medial map is crucial. In [17], authors use a map based on level sets that in spite of giving a normalized response it has two main weak points. On one side, the response is

a step-wise almost binary map that is prone to introduce internal surface holes in the further NMS stage. On the other side, the response significantly drops at surface branches, which, again, might introduce unconnected components.

The present work focuses on the definition of a medial map capable of producing complete medial surfaces reaching a good compromise between simplicity of the medial geometry and its ability to reconstruct the whole anatomical volume. We introduce a medial map based on ridge detectors that combines the advantages of steerable filters and level sets geometry. We call this medial map Geometric Steerable Medial Map, GSM2. A database of liver segmentations generated from an abdominal atlas [11,6] is used as a benchmark to evaluate the accuracy of volumes reconstructed from medial surfaces, as well as the capability for preserving medial main branches. Results show that the proposed GSM2 produces branching topologies related to anatomy concavities that have a reconstruction power higher than thinning approaches.

2 Medial Map Combining Geometric and Steerable Filters

Distance maps are a key element for obtaining medial maps, since, by definition, their maximum values are located at central voxels corresponding to the medial structure. Distance maps can be used directly to generate skeletons (see [10]) but the ridges of the distance map have show superior power to identify medial voxels [17]. In image processing, ridge detectors are based either on level sets geometry or image intensity profiles.

The operator described in [8] defines ridges as lines joining points of maximum curvature of the distance map level sets. It is computed using the maximum eigenvector of the structure tensor of the distance map as follows.

Let \mathbf{V} be the eigenvector of principal eigenvalue of the structure tensor and consider its reorientation along the distance gradient, $\mathbf{V} = (P, Q, R)$, given as:

$$\mathbf{V} = \text{sign}(\langle \mathbf{V} \cdot \nabla D \rangle) \cdot \mathbf{V}$$

for $\langle \cdot \rangle$ the scalar product. The ridgeness measure [8] is given by the divergence:

$$NRM := \text{div}(\mathbf{V}) = \partial_x P + \partial_y Q + \partial_z R \quad (1)$$

The above operator assigns positive values to ridge pixels and negative values to valley ones.

A main advantage is that $NRM \in [-N, N]$ for N the dimension of the volume. In this way, it is possible to set a threshold common to any volume for detecting significant ridges and, thus, points highly likely to belong to the medial surface. However, by its geometric nature, NRM has two main limitations. In order to be properly defined, NRM requires that the vector \mathbf{V} uniquely defines the tangent space to image level sets. Therefore, the operator achieves strong responses in the case of one-fold medial manifolds, but significantly drops anywhere two or more medial surfaces intersect each other. Additionally, NRM responses are not

continuous maps but step-wise almost binary images (see Fig. 2, left). Such discrete nature of the map hinders the performance of the NMS binarization step that removes some internal voxels of the medial structure and, thus, introduces holes in the final medial surface.

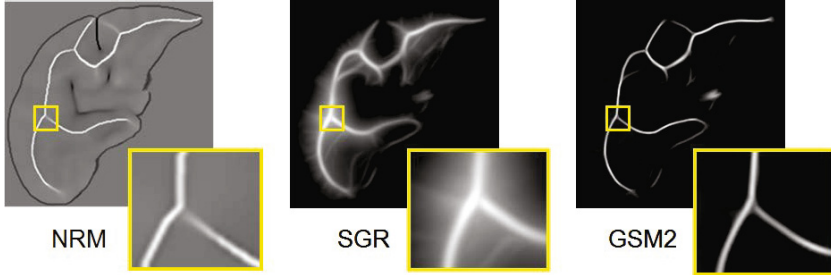


Fig. 2. Performance of different ridge operators. Normalized Ridge Map (left), Steerable Gaussian Ridge (center) and Geometric Steerable Medial Map (right).

On the other side, ridge maps based on image intensity are computed by convolution with a bank of steerable filters. Each filter is defined by 2nd derivatives of (oriented) anisotropic 3D Gaussian kernels:

$$g_{\sigma}^{\Theta} = g_{(\sigma_x, \sigma_y, \sigma_z)}^{(\theta, \phi)} = \frac{1}{(2\pi)^{3/2} \sigma_x \sigma_y \sigma_z} e^{-\left(\frac{\tilde{x}^2}{2\sigma_x^2} + \frac{\tilde{y}^2}{2\sigma_y^2} + \frac{\tilde{z}^2}{2\sigma_z^2}\right)}$$

for $(\tilde{x}, \tilde{y}, \tilde{z})$ the coordinates given by a rotations of angles θ and ϕ that transform the z-axis into the unitary vector $(\cos \phi \cos \theta, \cos \phi \sin \theta, \sin \phi)$. In order to detect sheet-like ridges, the scales are set to $\sigma_z < \sigma_x = \sigma_y$.

The second partial derivative along the z axis constitutes the principal kernel for computing ridges:

$$\partial_z^2 g_{\sigma}^{\Theta} = (\tilde{z}^2 / \sigma_z^4 - 1 / \sigma_z^2) g_{\sigma}^{\Theta}$$

The response of the operator Steerable Gaussian Ridge (SGR) is calculated as the maximum response for a discrete sampling of the angulation:

$$SGR := \max_{i,j} (D * \partial_z^2 g_{\sigma}^{\Theta_{i,j}}) \tag{2}$$

for $\Theta_{i,j}$ given by $\theta_i = \{\frac{i\pi}{N}, i = 1..N\}$ and $\phi_j = \{\frac{j\pi}{M}, j = 1..M\}$.

A main advantage of using steerable filters is that their response provides continuous maps which ensure completeness of the surfaces obtained by NMS binarization. Besides, since they decouple the space of possible orientations for medial surfaces, their response does not decrease at self-intersections (see Fig. 2, left and center). Their main counterpart is that their response is not normalized, so setting the threshold for NMS binarization becomes a delicate issue.

The analysis above shows that geometric and intensity methods have complementary advantages and shortcomings. Therefore we propose combining them into the following Geometric Steerable Medial Map (GSM2):

$$GSM2 := SGR(NMR) = \max_{i,j} (NRM * \partial_z^2 g_\sigma^{\Theta_{i,j}}) \quad (3)$$

The advantages of GSM2 are two-fold. On one hand, steerable filters provide a continuous approximation to NMR semi-discrete maps with a more uniform response at self-intersecting points. On the other hand, because NMR maps have a sharp response at central voxels, GSM2 still provides a highly selective response at ridges. In this manner GSM2 generates medial maps with good combination of specificity in detecting medial voxels while having good characteristics for NMS binarization, which does not introduce internal holes (Fig. 2, right).

3 Validation Experiments

In order to provide a real scenario for the reconstruction tests we have used an atlas of abdominal organs computed by normalized probabilistic models from the registration of 9 subjects [11,6]. By its higher concavity complexity we have chosen the liver as a source of anatomical volumes. We have applied GSM2 using $\sigma = 0.5$, $\rho = 1$ for computing structure tensors in NMR and $N = M = 8$ orientations for SGR. In order to check the capability of GSM2 for preserving medial main branching topology, we have considered the full surface as well as a simplified surface (labelled $GSM2_S$) obtained by removal of secondary medial branches. For comparison to morphological methods, we have also applied an ordered thinning using a 26-connected neighborhood [10] followed by a pruning (labelled Th_{26P}).

Figure 3 shows the three kinds of medial surfaces considered on a representative liver. In spite of pruning, medial manifolds computed using thinning have a branching geometry more complex than GSM2 and apparently not related to the volume boundary geometry (concave-convex profile). This is not the case for GSM2 surfaces, whose branching topology arises from volume boundary concavities. It follows that its subsequent simplification is better suited for volume convex decomposition, which naturally describe the geometry of objects [7].

Our experiments will focus on evaluating how the pruning affects the generation of reconstructed volumes. Volumes are reconstructed from the computed medial surfaces by applying the inverse medial transform. Comparisons with the original shape are based on volume overlap error (VOE) and maximum symmetric surface distances (MxSD) [4]. Lower metric values indicate better reconstruction capability: VOE provides a global score, while MxSD detects local deviations in the shape of the volume boundary.

Table 1 reports metric scores for each liver. For most livers, thinning is the worst performer in terms of reconstruction power and boundary distortion, while the complete GSM2 is the best method. It is worth noticing that the global volume reconstruction of the simplified GSM2 compares to its complete version

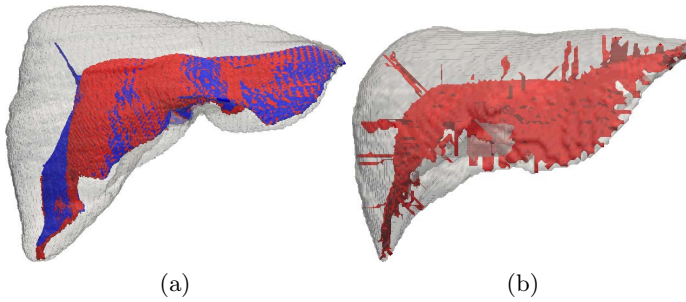


Fig. 3. Medial Manifolds of a healthy liver: full GSM2 (blue surface) and its simplification (red surface), (a) and Th_{26P} , (b)

in all cases. Regarding volume boundaries, we have a noticeable distortion in 3 cases (livers 2, 5 and 7). Distortion appears in the superior liver lobe due to a more prominent concavity in this lobe for the three cases (as illustrated in Fig. 4(a)). This might hinder proper measurements of abnormal or pathological structures. This is not the case for GSM2 complete surfaces as exemplified in Fig. 4. The oversized superior lobe on the right liver is captured by the presence of an unusual medial manifold configuration.

Table 1. Errors in reconstruction VOE and MxSD for each liver

	$GSM2$		$GSM2_S$		Th_{26P}	
	VOE	MxSD	VOE	MxSD	VOE	MxSD
Liver 1	2.51	8.37	2.78	8.37	3.14	12.04
Liver 2	2.22	9	2.85	12.41	2.60	10.68
Liver 3	2.58	8.78	2.92	8.78	3.13	12.04
Liver 4	2.51	9.80	2.55	9.85	2.84	10.77
Liver 5	2.42	4.24	2.83	8.60	2.73	9.64
Liver 6	2.49	9.27	2.71	9.27	2.69	7.49
Liver 7	2.25	4.90	2.69	10.20	2.73	10.48
Liver 8	2.12	10.44	2.36	10.44	2.41	10.77
Liver 9	2.72	9.69	2.98	9.69	3.05	12.04
Mean	2.42	8.28	2.74	9.73	2.81	10.66
Std Dev.	0.19	2.19	0.19	1.23	0.25	1.45

4 Conclusions

In order to provide manageable representations of complex organs, medial manifolds should reach a compromise between simplicity in geometry and capability

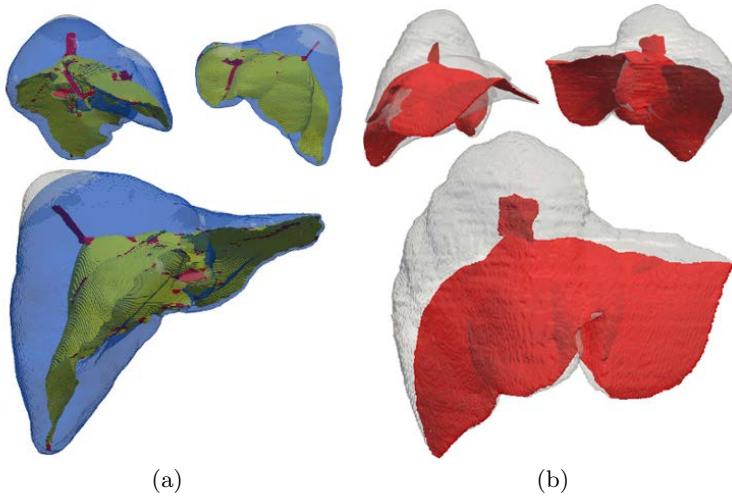


Fig. 4. Impact of medial branching topology: (a) reconstruction error for a healthy liver when using complete GSM2 (white volume and red surface) and simplified GSM2 (blue volume and yellow surface), and detection of unusual lobe for a pathological case, (b)

for restoring the anatomy of the organ. The method presented in this paper allows the computation of medial manifolds resulting in surfaces of greater simplicity than the generated by thinning methods. Although having this minimalistic property, the resulting manifolds can be used to recalculate the original volume with slightly better reconstructions than existing methods.

Our experiments show that our method is preferable to using a generic template since it allows tackling a wider set of shapes which could not be precisely represented by a generic manifold. Any simplification of a medial surface results in a drop in reconstruction quality. This drop in accuracy is hard to relate to the simplification process because the branching topology of thinning-based medial manifolds is not always related to the anatomy curvature (concavity-convexity pattern). A main advantage of GSM2 medial surfaces is that their branches are linked to the shape concavities due to the geometrical and normalized nature of the operator. In this context, GSM2 manifolds can be simplified (pruned) ensuring that the loss of reconstruction power will be minimum.

Future work includes the usage of GSM2 surfaces in the context of shape parametrization, providing a new set of coordinates to each point in the volume.

Acknowledgements. This research has been funded by the Spanish projects TIN2009-13618, CSD2007-00018 and 2009-TEM-00007. The last author has been supported by the Ramon y Cajal Program.

References

1. Blum, H.: A transformation for extracting descriptors of shape. MIT Press (1967)
2. Brechbuehler, C., Gerig, G., Kuebler, O.: Surface parametrization and shape description, pp. 80–89 (1992)
3. Gu, X., Wang, Y., Chan, T.F., Thompson, P.M., Yau, S.: Genus zero surface conformal mapping and its application to brain surface mapping. *IEEE TMI* 23(8), 949–958 (2003)
4. Heimann, T., van Ginneken, B., Styner, M.A., Arzhaeva, Y., Aurich, V.: Comparison and evaluation of methods for liver segmentation from CT datasets. *IEEE Trans. Med. Imag.* 28(8), 1251–1265 (2009)
5. Lee, T.C., Kashyap, R.L., Chu, C.N.: Building skeleton models via 3-D medial surface axis thinning algorithms. *Graph. Mod. Imag. Process.* 56(6), 462–478 (1994)
6. Linguraru, M.G., Sandberg, J.A., Li, Z., Shah, F., Summers, R.M.: Automated segmentation and quantification of liver and spleen from ct images using normalized probabilistic atlases and enhancement. *Medical Physics* 37(2), 771–783 (2010)
7. Liu, H., Liu, W., Latecki, L.J.: Convex shape decomposition. In: *CVPR*, pp. 97–104 (2010)
8. Lopez, A.M., Lumbreras, F., Serrat, J., Villanueva, J.J.: Evaluation of methods for ridge and valley detection. *IEEE Trans. Pat. Ana. Mach. Intel.* 21(4), 327–335 (1999)
9. Pizer, S.M., Thomas Fletcher, P.: Deformable M-Reps for 3D medical image segmentation. *Int. J. Comp. Vis.* 55(2), 85–106 (2003)
10. Pudney, C.: Distance-ordered homotopic thinning: A skeletonization algorithm for 3D digital images. *Comp. Vis. Imag. Underst.* 72(2), 404–413 (1998)
11. Reyes, M., González Ballester, M.A., Li, Z., Kozic, N., Chin, S., Summers, R.M., Linguraru, M.G.: Anatomical variability of organs via principal factor analysis from the construction of an abdominal probabilistic atlas. In: *IEEE ISBI*, pp. 682–685 (2009)
12. Stough, J.V., Broadhurst, R.E., Pizer, S.M., Chaney, E.L.: Regional Appearance in Deformable Model Segmentation. In: Karssemeijer, N., Lelieveldt, B. (eds.) *IPMI 2007*. LNCS, vol. 4584, pp. 532–543. Springer, Heidelberg (2007)
13. Styner, M., Gerig, G., Lieberman, J., Jones, D., Weinberger, D.: Statistical shape analysis of neuroanatomical structures based on medial models. *Medical Image Analysis* 7(3), 207–220 (2003); *Functional Imaging and Modeling of the Heart*
14. Styner, M., Lieberman, J.A., Pantazis, D., Gerig, G.: Boundary and medial shape analysis of the hippocampus in schizophrenia. *Medical Image Analysis* 8(3), 197–203 (2004)
15. Sun, H., Avants, B.B., Frangi, A.F., Sukno, F., Gee, J.C., Yushkevich, P.A.: Cardiac Medial Modeling and Time-Course Heart Wall Thickness Analysis. In: Metaxas, D., Axel, L., Fichtinger, G., Székely, G. (eds.) *MICCAI 2008, Part II*. LNCS, vol. 5242, pp. 766–773. Springer, Heidelberg (2008)
16. Sun, H., Frangi, A.F., Wang, H., Sukno, F.M., Tobon-Gomez, C., Yushkevich, P.A.: Automatic Cardiac MRI Segmentation Using a Biventricular Deformable Medial Model. In: Jiang, T., Navab, N., Pluim, J.P.W., Viergever, M.A. (eds.) *MICCAI 2010, Part I*. LNCS, vol. 6361, pp. 468–475. Springer, Heidelberg (2010)
17. Vera, S., Gil, D., Borràs, A., Sánchez, X., Pérez, F., Linguraru, M.G., González Ballester, M.A.: Computation and Evaluation of Medial Surfaces for Shape Representation of Abdominal Organs. In: Yoshida, H., Sakas, G., Linguraru, M.G. (eds.) *Abdominal Imaging 2011*. LNCS, vol. 7029, pp. 223–230. Springer, Heidelberg (2012)

18. Yushkevich, P.A.: Continuous medial representation of brain structures using the biharmonic PDE. *NeuroImage* 45(1), 99–110 (2009)
19. Yushkevich, P., Zhang, H., Gee, J.: Continuous medial representation for anatomical structures. *IEEE Trans. Medical Imaging* 25(12), 1547–1564 (2006)
20. Yushkevich, P.A., Zhang, H., Simon, T.J., Gee, J.C.: Structure-specific statistical mapping of white matter tracts. *NeuroImage* 41(2), 448–461 (2008)